

Convergent synaptic inputs to layer 1 cells of mouse cortex

Ying-Wan Lam  | S. Murray Sherman 

Department of Neurobiology, University of Chicago, Chicago, Illinois

Correspondence

S. Murray Sherman, Department of Neurobiology, University of Chicago, Chicago, IL.
Email: ywlam@uchicago.edu

Funding information

National Institute of Neurological Disorders and Stroke, Grant/Award Number: NS094184; National Eye Institute, Grant/Award Number: EY022388

Abstract

We used whole cell recordings from slice preparations of mouse cortex to identify various inputs to neurons of layer 1. Two sensory cortical areas were targeted: a primary somatosensory area, namely, the barrel cortex of S1, and a higher order visual area, namely, V2M. Results were similar from both areas. By activating local inputs using photostimulation with caged glutamate, we also identified glutamatergic (and possibly GABAergic) inputs from all lower layers plus GABAergic inputs from nearby layer 1 neurons. However, the patterns of such inputs to layer 1 neurons showed great variation among cells. In separate experiments, we found that electrical stimulation of axons running parallel to the cortical surface in layer 1 also evoked a variety of convergent input types to layer 1 neurons, including glutamatergic “drivers” and “modulators” plus classic modulatory inputs, including serotonergic, nicotinic, α - and β -adrenergic, from subcortical sites. Given that these layer 1 cells significantly affect the responses of other cortical neurons, especially via affecting the apical dendrites of pyramidal cells so important to cortical functioning, their role in cortical processing is significant. We believe that the data presented here lead to better understanding of the functioning of layer 1 neurons in their role of influencing cortical processing.

1 | INTRODUCTION

Layer 1 of the cortex consists of a dense neuropil including sparsely distributed GABAergic neurons (Winer & Larue, 1989). Axons innervating layer 1 include corticocortical, mostly consisting of feedback from higher areas (Cauller, Clancy, & Connors, 1998; D'Souza & Burkhalter, 2017; Marques, Nguyen, Fioreze, & Petreanu, 2018) and thalamocortical afferents from what Jones (Jones, 1998) has termed “matrix” thalamus (Avendano, Stepniewska, Rausell, &

Reinoso-Suarez, 1990; Cruikshank et al., 2012; Jones, 1998; Rubio-Garrido, Perez-de-Manzo, Porrero, Galazo, & Clasca, 2009). Interactions of these afferents and the roles they play in brain function have recently received much attention. For instance, recent work has implicated these inputs in processing of cross-modal and contextual information (Ibrahim et al., 2016; Roth et al., 2016). Despite this interest in layer 1 and after some earlier electrophysiological studies (Zhou & Hablitz, 1996a,b, 1997), there has been a remarkable lack of research into circuitry involving neurons of cortical layer 1. For instance, many models of cortical circuitry, including suggestions of “canonical” cortical circuits, ignore layer 1 cells (e.g., Douglas & Martin, 1991; Potjans & Diesmann, 2014).

These layer 1 neurons have been described as quite heterogeneous as regard to electrophysiological and morphological properties (Chu, Galarreta, & Hestrin, 2003; Jiang, Wang, Lee, Stornetta, & Zhu, 2013; Wozny & Williams, 2011), and they are innervated by strong “driver” like thalamocortical

Abbreviations: ACSF, artificial cerebrospinal fluid; AP5, D,L-2-amino-5-phosphonopentanoate; DNDS, 4,4'-dinitro-stilbene-2,2'-disulphonic acid; DNQX, 6,7-dinitroquinoxaline-2,3-dione; EPSC, excitatory postsynaptic current; GABA, gamma-aminobutyric acid; IPSC, inhibitory postsynaptic current; mGluR, metabotropic glutamatergic receptors; MPEP, methyl-6-(phenylethynyl)pyridine; S1, primary somatosensory cortex; TTX, tetrodotoxin; UV, ultraviolet; V2M, medial secondary visual cortex.

Edited by Paul Bolam. Reviewed by W. Usrey.

All peer review communications can be found with the online version of the article.

and corticocortical axons running in layer 1 (Cruikshank et al., 2012). Many of these interneurons form reciprocal GABAergic and electrical connections among themselves (Chu et al., 2003) and they provide inhibitory input to apical tufts of layers 2/3 and 5 pyramidal cells and to other cells of layers 2/3, forming different types of canonical microcircuits with neurons in these layers (Jiang et al., 2013; Lee et al., 2015; Wozny & Williams, 2011). Clearly, these layer 1 cells are in a position to significantly affect cortical functioning, and so it is critical that we extend our understanding of the full nature of inputs they integrate.

In this study, we used a combination of photostimulation, electrophysiology, and pharmacological agents to characterize the inputs to layer 1 neurons in primary and higher sensory cortices of mice. We showed that layer 1 neurons received convergent inputs of a variety of transmitter types. In addition to evidence of nicotinic (Christophe et al., 2002) and layer 2/3 inputs (Jiang et al., 2013; Lee et al., 2015; Wozny & Williams, 2011), we found glutamatergic and possibly GABAergic inputs from all lower layers, GABAergic inputs from nearby layer 1 cells, and inputs from axons running in layer 1 that include glutamatergic afferents as well as those of serotonergic, nicotinic, α - and β -adrenergic origins, presumably long-range projections from subcortical neuromodulator systems. Thus, like neurons in other cortical layers, these layer 1 neurons seem embedded in complex circuits that include local inputs, longer-range inputs from other cortical areas and/or thalamus, and from various classic modulator systems.

2 | METHODS

2.1 | Slice preparation

Our protocols followed the animal care guidelines of the University of Chicago. Adult (>6 weeks old) or adolescent (12–29 days postnatal) BALB/c mice (Harlan-Envigo) of both sexes were deeply anesthetized by inhalation of isoflurane, and their brains were quickly removed, immediately chilled in ice-cold artificial cerebrospinal fluid (ACSF) that contained (in mM): 125 NaCl, 3 KCl, 1.25 NaH₂PO₄, 1 MgCl₂, 2 CaCl₂, 25 NaHCO₃, 25 glucose, and cut at coronal plane into 500 μ m slices using a vibrating tissue slicer (Leica VT1000S). Slices that contained V2M or barrel cortex (abbreviated as S1 below) were identified by anatomical landmarks and then transferred to a holding chamber containing continuously oxygenated ACSF and incubated at room temperature for at least 1 hr until experiment.

2.2 | Photostimulation

We used our previously described methods for photostimulation (Lam & Sherman, 2005, 2007, 2010, 2011, 2015).

Briefly, data acquisition and photostimulation were controlled by the program Tidalwave (Shepherd, Pologruto, & Svoboda, 2003) written in Matlab (MathWorks, Natlick, MA, USA). Nitroindoliny (NI)-caged glutamate (Sigma-Aldrich, St Louis, MO, USA; Canepari, Nelson, Papageorgiou, Corrie, & Ogden, 2001) was added to the recirculating ACSF to a concentration of 0.39 mM during recording. Focal photolysis of the caged glutamate was accomplished by a pulsed UV laser (355 nm wavelength, frequency-tripled Nd:YVO₄, 100 kHz pulse repetition rate; DPSS Laser, San Jose, CA, USA). The laser beam was directed into the side port of a double-port tube (U-DPTS) on top of an Olympus microscope (BX50WI) using UV-enhanced aluminum mirrors (Thorlabs, Newton, NJ, USA) and a pair of mirror-galvanometers (Cambridge Technology, Cambridge, MA, USA) and then focused onto the brain slice using a low-magnification objective (4x0.1 Plan, Olympus). Angles of the mirror-galvanometers were computer controlled and determined the position stimulated by the laser. The Q-switch of the laser and a shutter (LS3-ZM2; Vincent Associate, Rochester, NY, USA) controlled the timing of the laser pulse for stimulation.

A variable neutral density wheel (Edmund, Barrington, NJ, USA) controlled the power of photostimulation at different levels during experiments by attenuating the intensity of the laser. A microscope coverslip in the laser path reflected a small portion of the laser onto a photodiode, and the current output from this photodiode was used to monitor the laser intensity during the experiment. The photodiode output was calibrated to the laser power at the back focal plane of the objective during setup of the optical equipment, using a power meter (Thorlabs, Newton, NJ, USA).

The standard stimulation pattern used for mapping consisted of positions arranged in a 16 \times 16 array (Figure 1c₁). To avoid receptor desensitization, local caged-glutamate depletion, and possible excitotoxicity, stimulation of these positions were arranged in a sequence that maximized the spatial distance between consecutive trials. The laser stimulus was 2 ms long and consisted of 200 pulses. Power used for laser varied between 75 and 80 mW measured at the back focal plane but as the transmittance of the objective for the UV laser was about 40%, the actual power of the laser reaching the slices was less than half of these values. The inter-trial-interval was between 1 and 2 s. A typical mapping experiment lasted between 30 min to an hour and we did not see any change of the response amplitude or membrane resistance during experiments that suggested damage from phototoxicity.

2.3 | Physiological recording

We recorded from 65 V2M and 40 S1 neurons following previously reported procedures (Cox & Sherman, 2000;

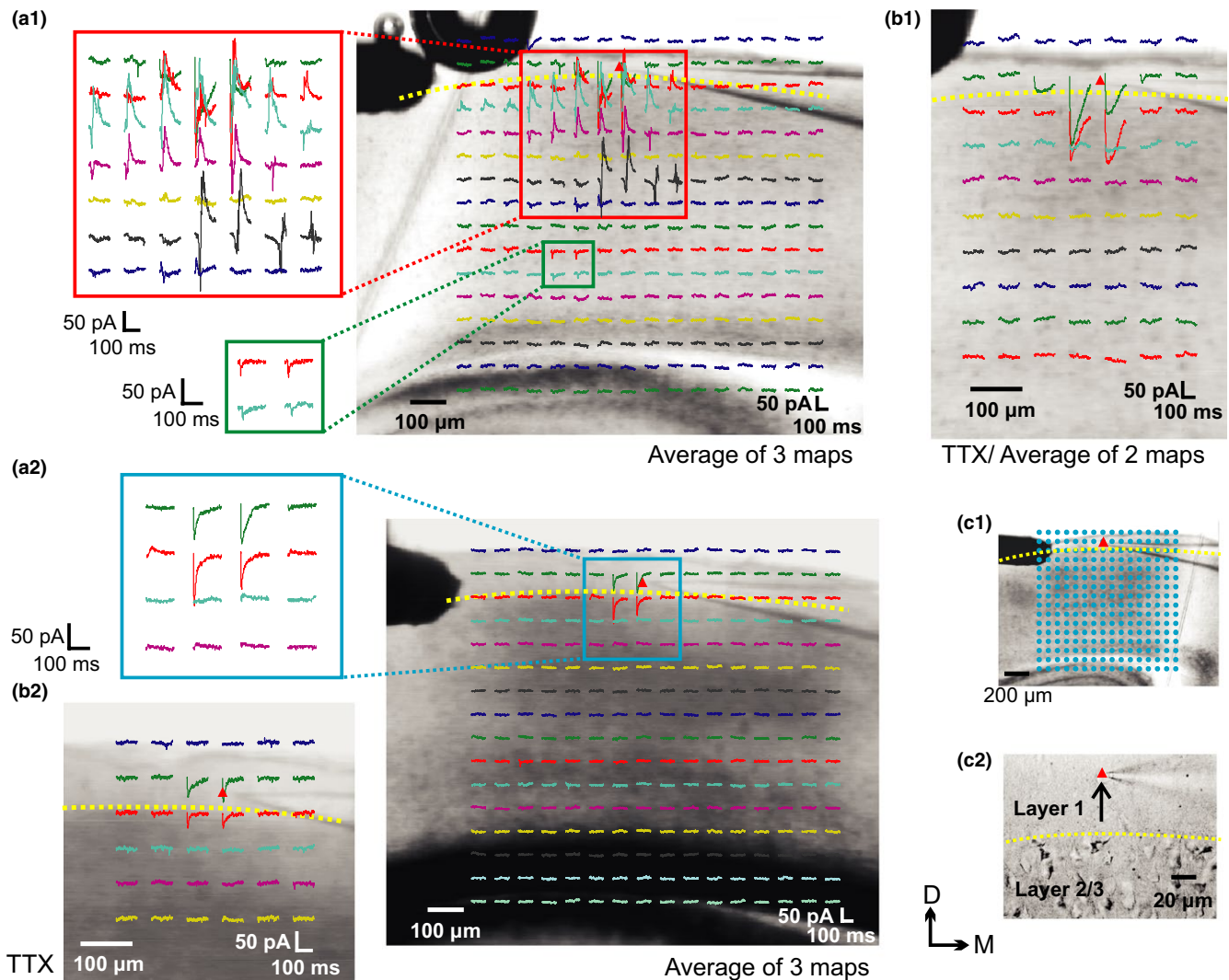


FIGURE 1 Responses of V2M layer 1 neurons to cortical photostimulation. (a) Layer 1 neurons (red triangles) were recorded in voltage-clamp mode while V2M was stimulated in all layers using UV laser in 256 positions. Recordings of the response were rearranged as square or rectangular grid and overlaid, on top a photomicrograph of the cortex taken during the experiment, at where the laser was focused (see Section 2). Selected regions where photostimulation evoked detectable responses were magnified and displayed at larger scales on the left (color squares). Yellow dotted line indicates the border between layer 1 and layer 2/3. (b) Responses of the same neurons to photostimulation around the recording site after all synaptic responses were inhibited by $1 \mu\text{M}$ TTX. (a₁,b₁) A neuron in which photostimulation evoked biphasic or outward current responses. (a₂,b₂) A neuron in which photostimulation evoked very little detectable synaptic responses, as shown by the similarity of the maps before (Figure 2a₂) and after (Figure 2b₂) TTX application. (c) Experimental setup. (c₁) A photomicrograph taken during an experiment showing placement of the concentric bipolar stimulating electrode and the pattern of photostimulation. (c₂) A photomicrograph taken at 40 \times that illustrates the criteria for layer 1 neurons selection

Lam, Cox, Varela, & Sherman, 2005). Experiments were conducted mostly on adolescent animals (12–29 days postnatal), although data of the mapping experiments from 10 V2M neurons of adult animals (>6 weeks postnatal) were also included and presented in Figures 1 and 3. Briefly, pipettes that had a tip resistance of 4–8 M Ω when filled with a low chloride solution were pulled from borosilicate glass capillaries using a horizontal puller (Sutter Instrument, P-87). Composition of the intracellular solution (in mM): 127 K-gluconate, 3 KCl, 1 MgCl₂, 0.07 CaCl₂, 10 HEPES, 2

Na₂-ATP, 0.3 Na-GTP, 0.1 EGTA was chosen so that the chloride reversal potential was low enough to facilitate detection of IPSCs when the neurons were held at -45 mV (Lam & Sherman, 2015). The pH of the pipette solution was adjusted to 7.3 with KOH or gluconic acid, and the osmolality was 280–290 mOsm. A few threads of nylon filaments, attached to a platinum wire slice holder, were used to secure the slices in the bath during recording. The slices were perfused with ACSF at 27 $^{\circ}\text{C}$ and all antagonists, except for 4,4'-dinitro-stilbene-2,2'-disulphonic acid

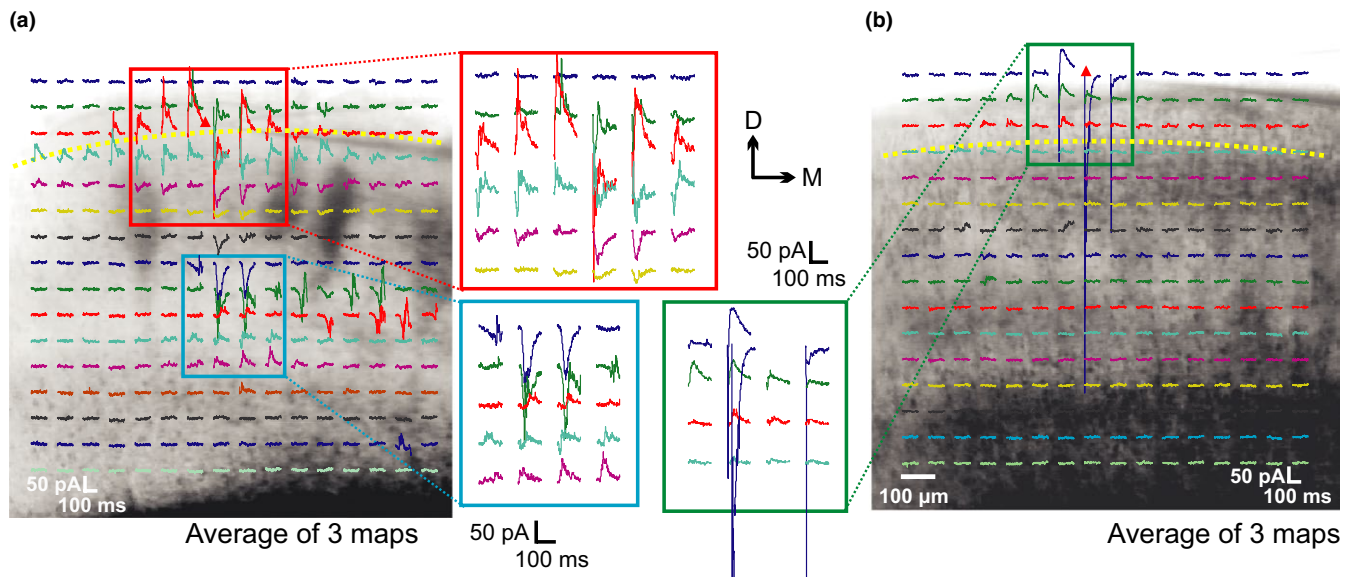


FIGURE 2 Responses of S1 layer 1 neurons to cortical photostimulation. (a,b) Layer 1 neurons (red triangles) were recorded in voltage-clamp mode while S1 was stimulated in all layers using UV laser in 256 positions. Recordings of the responses were displayed in the same format as Figure 1. Selected regions where photostimulation evoked detectable responses were magnified and displayed at larger scales (color squares and rectangles). Yellow dotted line indicates the border between layer 1 and layer 2/3. (a) An example in which photostimulation evoked excitatory or biphasic synaptic responses from large areas in upper and lower layers. (b) Another example in which photostimulation evoked detectable responses from only a small area around the soma

(DNDS), were bath applied; DNDS was applied by including it in the intracellular solution. Neurons were recorded using a visualized setup equipped with an Olympus microscope (BX50WI). V2M and S1 were located in the slices by anatomical landmarks. Specifically, V2M is identified as the cortical region closed to the midline, medial to the visual cortex (V1) in caudal coronal sections (Paxinos & Watson, 2008), and S1 is located by virtue of its distinctive barrel formations. Layer 1 neurons were visually selected under the microscope at 40X as the sparsely distributed cells located dorsal to the densely packed somata of layers 2/3 (Figure 1c₂). Data were recorded using an Axopatch 200B amplifier (Molecular Devices, Sunnyvale, CA, USA) controlled by the program Tidalwave (Shepherd et al., 2003).

All neurotransmitter antagonists were purchased from Tocris (Minneapolis, MN, USA). Other chemicals were obtained from Sigma-Aldrich.

2.4 | Data analysis

Responses to photostimulation could be easily and best detected visually by their short latency and the presence of similar responses in adjacent stimulation locations. These responses were averaged and analyzed using programs written in Matlab (Natick, MA, USA). For data presentation, traces of the recording immediately after the laser pulse were superimposed on a photomicrograph of the slice (see Section 3). For Figures 1 and 2, the abovementioned traces were arranged

into a square or rectangular array and placed where the laser was focused during the stimulation. In Figure 3, a summary of the results is plotted as pseudocolor maps with the amplitude of peak EPSCs and IPSCs represented by intensity of green and red colors, respectively; the locations where biphasic responses were evoked are represented by yellow pixels in such maps.

Paired-pulse effects were measured by comparing the height of the peak EPSCs relative to 5 ms baseline prior to electrical stimulation (distance between dotted lines in Figure 4b₂). Sizes of the slow inward current response to electrical stimulation are measured from the area above the response traces after the stimulus artifacts and high frequency noise were removed numerically by a 50 Hz low-pass Butterworth (Figures 5–7). Data points are plotted as means \pm SEM (standard error of means) in Figures 4–7 and statistical comparisons were performed using the Wilcoxon Rank test.

3 | RESULTS

3.1 | Convergent and heterogeneous topography for intra- and interlaminar inputs to layer 1 neurons

Intra- and interlaminar inputs to V2M layer 1 neurons were investigated using photostimulation with caged glutamate, which has the advantage of stimulating only somata and dendrites without affecting axons of passage. Data were obtained

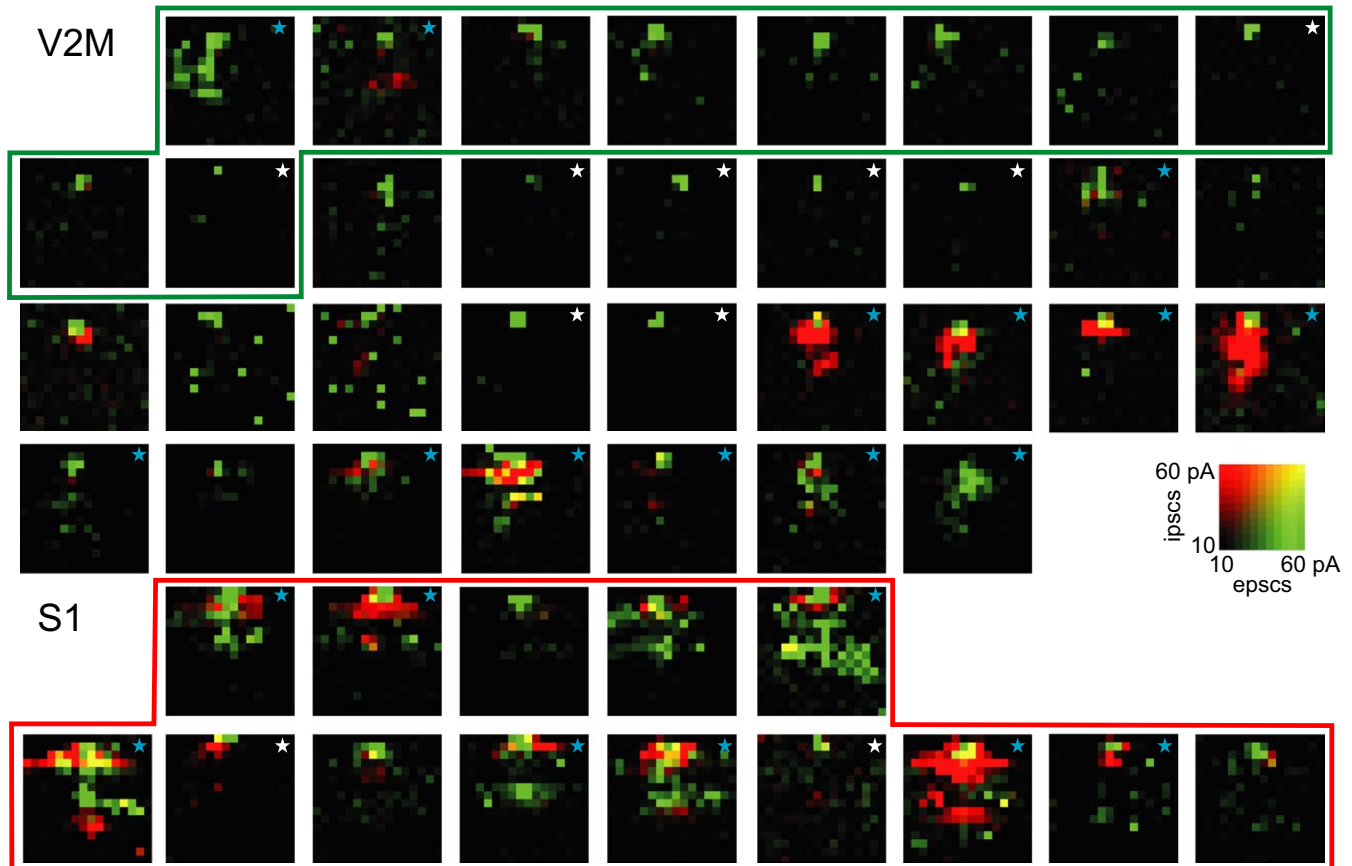


FIGURE 3 Spatial patterns of the cortical input to V2M and S1 layer 1 neurons. Peak EPSCs and IPSCs responses of layer 1 neurons to photostimulation were measured and represented by intensity of green and red colors, respectively, in pseudocolor maps. Locations where biphasic responses were evoked are represented by yellow pixels (see color scale). Blue stars indicate neurons that receive extensive upper and lower laminar inputs and white stars indicate those receiving little or no synaptic inputs. Results from adult V2M slices are encircled by a green line and maps of S1 neurons are encircled by a red line

from 10 adult (>6 weeks postnatal) and 23 adolescent (12–29 days postnatal) mice. We did not detect any differences in the input maps from these two age groups; data from the two age groups are documented together below in Figures 1 and 3.

Figure 1 shows two such experiments in which inputs to layer 1 neurons were photostimulated at 256 locations. Recorded traces were averaged, rearranged as square or rectangular arrays and overlaid on a photomicrograph taken during the experiment, and the traces thus were placed at locations where the laser was focused (see Section 2). In Figure 1a₁,a₂, traces with detectable synaptic responses were placed within red or blue rectangles. The areas where photostimulation directly depolarized the dendrites and somata of these neurons, after all synaptic responses were blocked by 1 μ M of TTX, are displayed in Figure 1b₁,b₂ to illustrate the approximate extent of their dendritic arbors. Figure 1a₁,b₁ shows the results from an example neuron in which biphasic EPSC/IPSCs (upper layers) or EPSCs (lower layer) responses were evoked by photostimulation in a large area of V2M. The

responses before and after TTX application were very similar for another example shown in Figure 1a₂,b₂, suggesting that photostimulation evoked very little in the way of synaptic currents in this condition.

Similar experiments were repeated in 14 S1 layer 1 neurons of adolescent mice (13–27 days postnatal). The results from two experiments are presented in Figure 2 in a similar format as Figure 1a₁,a₂. In the first example shown in Figure 2a, photostimulation of large areas in upper and middle layers of cortex evoked large excitatory or biphasic synaptic responses, suggesting that the cell receives extensive synaptic inputs from these layers. Figure 2b shows another example in which photostimulation evoked detectable responses from only a small area around the soma.

Results from all 47 experiments are summarized as pseudocolor maps in Figure 3. Peak inward (EPSCs) and outward (IPSCs) currents were measured from the averaged responses to photostimulation and represented as different intensities of green and red colors, respectively, and biphasic responses are shown as yellow pixels (color scale, Figure 3).

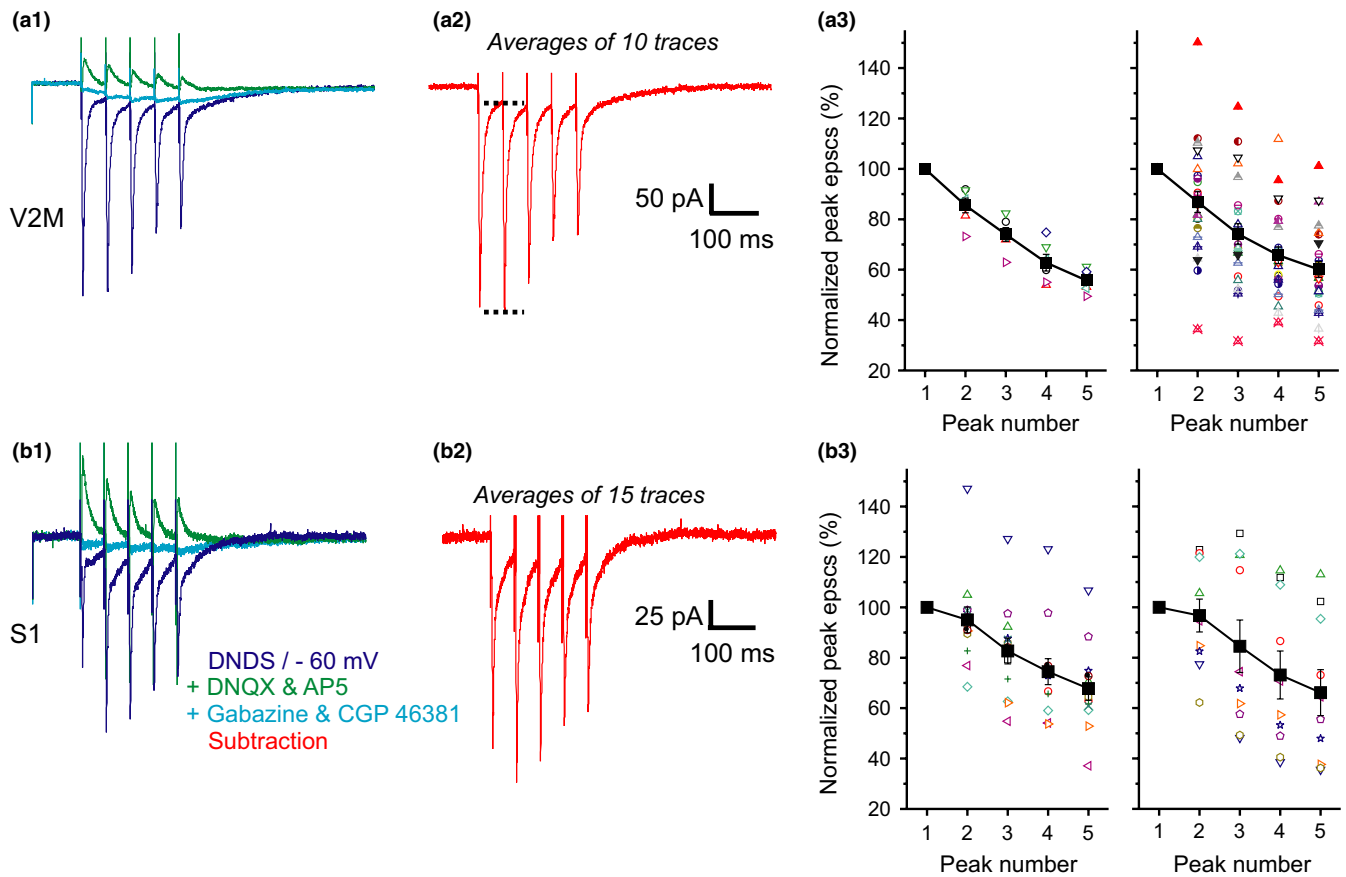


FIGURE 4 (a,b) Glutamatergic EPSCs evoked by electrical stimulation of layer 1 fibers are paired pulse depressing. (a₁,b₁) Example responses (violet) of layer 1 neurons, recorded with 1 mM DNDS included in the intracellular solution, to five electrical stimulations delivered at 20 Hz from a concentric bipolar electrode placed in layer 1. Green traces show the average responses after bath applications of AMPA and NMDA antagonists. Blue traces show the remaining slow inward currents after further blockade of GABA_A and GABA_B currents. (a₂,b₂) Glutamatergic (AMPA & NMDA) currents calculated mathematically by subtracting the green traces from the violet traces in figure a₁,b₁. Dotted lines in figure a₂ indicate how the peak heights of EPSCs were measured. (a₃,b₃) Summary graphs showing pair pulse effects across experiments. Normalized peak EPSCs are plotted against the stimulus numbers. The averages across experiments are represented as solid squares (means \pm SEM) and results from individual experiments are shown as symbols in different shapes and colors. Left: Experiments in which glutamatergic and GABAergic antagonists were applied in sequence and the sum of AMPA and NMDA currents were calculated using the method described in figure a₂ and b₂. Right: Experiments in which glutamatergic and GABAergic antagonists were simultaneously applied and the glutamatergic responses in these experiments were approximated by subtracting the slow inward current remained (blue traces in figure a₁ and b₁) from the original responses (violet)

The topography of intralaminar and lower laminar inputs to the recorded layer 1 neurons vary widely among different neurons. Layer 1 neurons that received extensive synaptic inputs from lower layers are indicated with blue stars in Figure 3 and neurons in which photostimulation evoked responses from only a small area, probably little larger than the size of their dendritic arbor and immediately surrounding the recording site, are indicated with white stars (Figure 3).

3.2 | Strong “driver-like” layer 1 inputs to layer 1 interneurons

Responses to electrical stimulation of layer 1 axons were tested in 32 V2M and 23 S1 layer 1 neurons from adolescent

mice (13–29 days postnatal) using a concentric bipolar stimulating electrode placed laterally to the recording sites (Figure 1c₁). Stimulation from these electrodes usually evoked biphasic responses that were composed of overlapping EPSCs and IPSCs. Examples of such responses to five, 20 Hz, 0.2 ms duration pulses after the IPSCs were partially inhibited by a GABA_A blocker (1 mM DNDS) included in the pipette solution, are shown in Figure 4a₁ (V2M, violet) and Figure 4b₁ (S1, violet). Application of AMPA (50 μ M 6, 7-dinitroquinoxaline-2,3-dione, DNQX) and NMDA (50 μ M D,L-2-amino-5-phosphonopentanoate, AP5) antagonists abolished the glutamatergic currents (Figure 4a₁,b₁, green), and the responses that remained consisted of small outward currents, which were inhibited by the additional placement

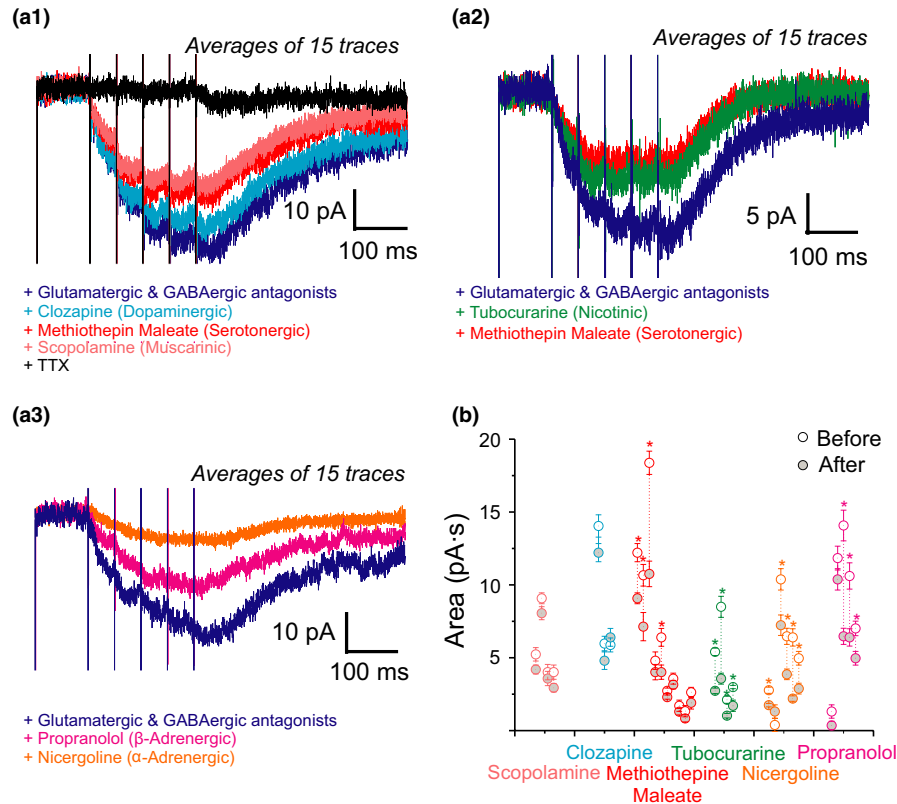


FIGURE 5 Slow inward current electrically evoked by 20 Hz (five pulses) stimulation in V2M layer 1 neurons was inhibited by different neuromodulator antagonists. (a₁₋₃) Example experiments in which neuromodulators antagonists were bath applied in sequence. Antagonists and their application order are color-coded and listed in legends below the traces. (a₁) An experiment in which serotonergic antagonist methiothepin maleate (red) suppressed the slow current while dopaminergic (clozapine, blue) and muscarinic (scopolamine, pink) antagonists had very little effects. The slow current was completely abolished in the presence of TTX (black). (a₂) Tubocurarine, a nicotinic antagonist, inhibited the slow current (green) and methiothepin maleate (serotonergic, red) had only a small effect in this experiment. (a₃) The slow current was inhibited by the antagonists of both α - (magenta) and β -adrenergic (orange) receptors in this experiment. (b) Graphic summary of the effects of all neuromodulator antagonists. Total area above filtered response traces (50 Hz low pass Butterworth) in trials before (open circles) and after (gray-filled circles) drug application were measured, averaged and plotted (means \pm SEM) as circles connected with dotted lines. Significant differences between the responses before and after drug application (Wilcoxon Rank test, $p < 0.05$) are indicated with asterisks

of GABAergic antagonists (25 μ M Gabazine and 30 μ M CGP46381) in the bath; what remained after glutamatergic and GABAergic responses were abolished was a small, slow inward current (blue).

Glutamatergic responses in 6 V2M and 13 S1 neurons were estimated by calculating the difference between before (violet) and after (green) application of glutamatergic antagonists, because the GABAergic currents were not completely inhibited at the concentration of DNDS we used; results of such estimates are displayed in Figure 4a₂,b₂. The amplitudes of the peak glutamatergic EPSCs were measured as the distance between the dotted lines shown in Figure 4a₂. These amplitudes were then normalized and plotted in Figure 4a₃,b₃ against the pulse number in the stimulation train (left panels). In the other 26 V2M and 10 S1 neurons, glutamatergic and GABAergic antagonists were applied simultaneously and the glutamatergic EPSCs

were estimated by subtracting the slow current remained after drugs application (Figure 4a₁,b₁, blue) from the original responses (Figure 4a₁,b₁, violet). The peak EPSCs from these experiments were calculated and plotted similarly in the right panels of Figure 4a₃,b₃. Glutamatergic inputs to V2M and S1 layer 1 stimulation, estimated by both methods, show clear paired-pulse depression.

3.3 | Classical neuromodulator inputs to layer 1 neurons

From 19 V2M neurons and 17 S1 neurons recorded in layer 1, we managed to further investigate the slow inward current remaining after application of glutamatergic and GABAergic antagonists (blue traces in Figure 4a₁,b₁).

V2M neurons were stimulated by five electrical pulses delivered at 20 Hz when antagonists of various neurotransmitters

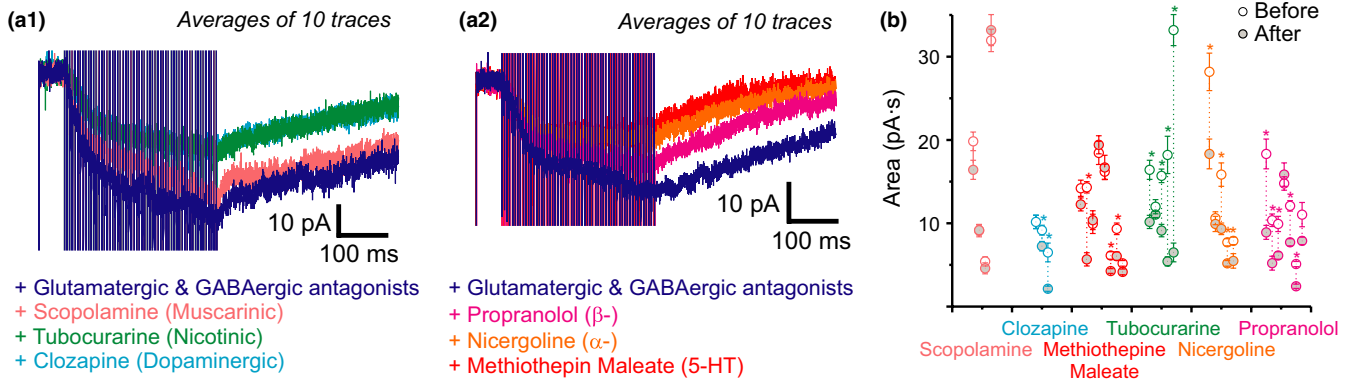


FIGURE 6 Slow electrically inward current evoked in S1 layer 1 neurons was inhibited by different neuromodulator antagonists. (a_{1&2}) Example experiments in which neuromodulators antagonists were bath applied in sequence while layer 1 neurons were stimulated at 200 Hz for 300 ms. Similar to Figure 5a, antagonist and their application sequences are specified by color-coded legends below the traces. (a₁) Nicotinic antagonist, tubocurarine (green), suppressed the slow current while muscarinic, scopolamine (pink), and dopaminergic, clozapine (blue, behind the green trace) antagonists had little effect. (a₂) α - (magenta) and β -adrenergic (orange) antagonists suppressed the slow inward current while serotonergic only slightly decreased its size. (b) Graphic summary of the effects of all neuromodulator antagonists across experiments. Total area above filtered response traces (50 Hz low pass Butterworth) before (open circles) and after (gray-filled circles) drug application were measured, averaged, and plotted (means \pm SEM) in a format similar to Figure 5b. Asterisks indicate significant differences between the responses before and after drug application (Wilcoxon Rank test, $p < 0.05$)

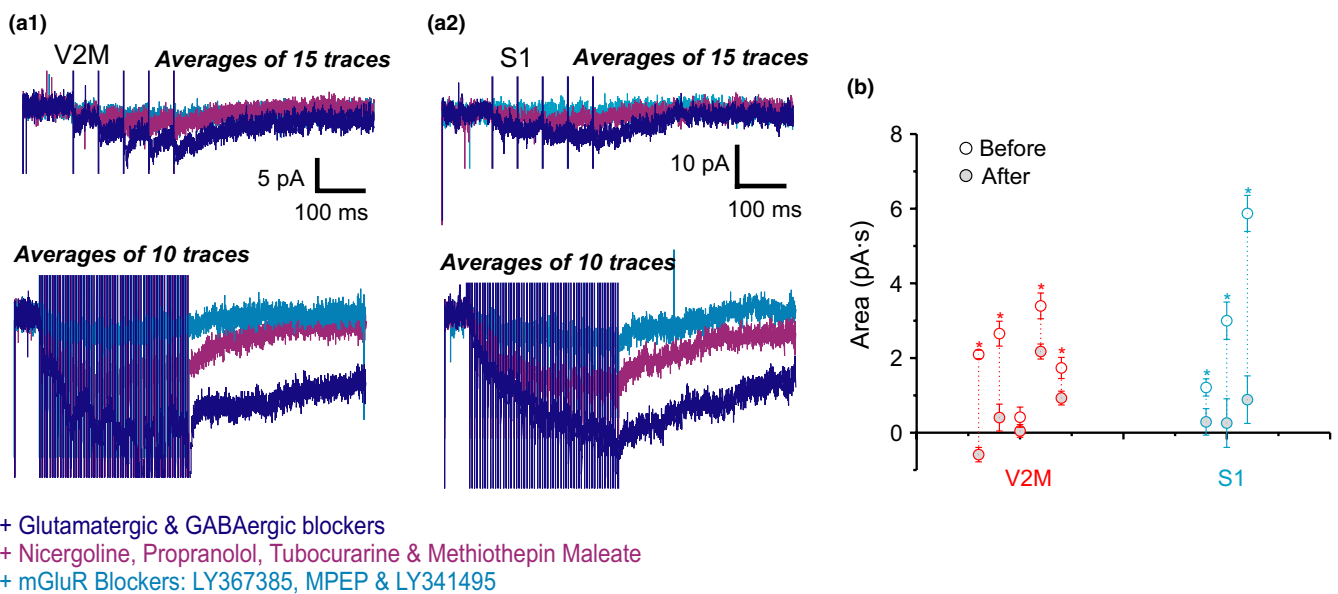


FIGURE 7 Effects of mGluR antagonists on the electrically evoked slow inward current in layer 1 neurons. (a_{1&2}) Example experiments showing the effects of mGluR antagonists for V2M (figure a₁) and S1 (figure a₂) layer 1 neurons when they were stimulated at 20 Hz (top) and 200 Hz (bottom). Application of a cocktail of mGluR antagonists (blue) produced visible reduction of the slow current after the responses involving other neurotransmitters were inhibited (purple). (b) Graphic summary of the effects of mGluR antagonists on responses evoked by 200 Hz stimulation, plotted in a format similar to Figure 5b. Asterisks indicate experiments with significant differences between the responses before and after drug application (Wilcoxon Rank test, $p < 0.05$)

were bath applied in sequence. Figure 5a₁₋₃ shows the results from three such cells recorded in V2M. Response traces from trials before and after antagonist application are averaged and plotted in color. The color-coded legends below list the antagonists tested and their application order.

Figure 5a₁, shows an experiment in which we tested the effects of dopaminergic (10 μ M clozapine, blue), serotonergic (10 μ M methiothepin maleate, red), and muscarinic (10 μ M scopolamine, pink) antagonists. Application of 1 μ M TTX in this neuron completely abolished the slow inward current,

TABLE 1 Effects of antagonists on the slow electrically evoked current in layer 1 neurons

	10 μ M Clozapine	10 μ M Methiothepin Maleate	10 μ M Scopolamine	10 μ M Tubocurarine	10 μ M Nicergoline	10 μ M Propranolol	1 μ M TTX
V2M	0/3 0.056 0.213 0.648	4/10 <0.001 0.002 <0.001 0.004 0.089 0.383 0.481 0.455 0.407 0.362	0/4 0.121 0.068 0.455 0.106	4/4 <0.001 <0.001 0.003 0.011	5/6 <0.001 <0.001 <0.001 0.002 0.004 0.115	3/5 <0.001 <0.001 0.010 0.089 0.213	3/3 <0.001 <0.001 <0.001
S1	2/3 0.004 0.038 0.970	3/8 <0.001 0.002 0.007 0.162 0.910 0.385 0.791 0.104	0/4 0.076 0.427 0.571 1.000	4/5 <0.001 0.002 <0.001 <0.001 0.791	4/5 0.001 0.002 <0.001 0.007 0.521	5/7 <0.001 0.001 0.002 <0.001 <0.001 0.141 0.734	—

Note. Numbers of experiments in which the slow current were significantly suppressed (Wilcoxon Rank test) and the *p* values (italics) of all comparisons are listed in the table. Significant *p* values are marked in bold.

demonstrating that it is of synaptic origin. Experiments shown in Figure 5a_{2,3} tested the effects of nicotinic (10 μ M tubocurarine, green), serotonergic (red), β - (10 μ M propranolol, magenta), and α -adrenergic (10 μ M nicergoline, orange) antagonists, respectively.

The areas above the filtered (50 Hz low pass Butterworth) traces before and after drug application in all tested V2M neurons were measured, averaged, and plotted in Figure 5b. Here, the responses (mean \pm SEM) before and after drug application are represented as open and gray-filled circles, respectively; experiments in which the responses were significantly suppressed (Wilcoxon Rank test, $p < 0.05$) are marked with asterisks (Figure 5b). The numbers of experiments in which antagonist application significantly reduced the slow current response and the *p* values of all statistical comparisons are listed in Table 1. Nicotinic (4/4) and α -adrenergic (5/6) antagonists significantly inhibited the responses in all or almost all experiments. Serotonergic (4/10) and β -adrenergic (3/5) antagonist reduced the slow current in roughly half of the neurons. Dopaminergic (0/3) and muscarinic (0/4) antagonists had no effects in all tested neurons. TTX abolished the slow current in all three experiments.

Similar experiments were performed in 17 S1 neurons stimulated at 200 Hz for 300 ms, a stimulation protocol that evoked larger inward current responses. Figure 6a₁₋₂ displays the results from two such experiments in a similar format as Figure 5. Experiment shown in Figure 6a₁ tested the effects of muscarinic, nicotinic, and dopaminergic antagonists, and the experiment in Figure 6a₂ tested the effects of serotonergic, β - and α -adrenergic antagonists.

As in Figure 5b, the areas above the filtered responses were measured, averaged, and plotted in Figure 6b. Experiments in which the responses before and after drug application were significantly different (Wilcoxon Rank test, $p < 0.05$) are also indicated with asterisks in the figure. The effects of all antagonists and the *p* values of all comparisons are also listed in Table 1. Similar to V2M neurons, nicotinic (4/4), serotonergic (3/8), α - (4/5), and β -adrenergic (5/7) antagonists significantly inhibited the responses in some or all of the experiments. Muscarinic antagonist (0/4) had no effect on the slow current. Unlike V2M neurons, however, dopaminergic antagonist, clozapine, reduced the response in two of the three tested S1 neurons (Table 1).

3.4 | Metabotropic glutamatergic inputs to layer 1 neurons

The effects of metabotropic glutamatergic antagonists were tested in 5 V2M and 3 S1 neurons and Figure 7a₁₋₂ shows two examples. The neurons were stimulated at either 20 Hz (top) or 200 Hz (bottom) and antagonists were applied to suppress most known neurotransmitter currents (purple) before the effect of a cocktail of mGluR blockers (50 μ M LY367385,

30 μM 2-methyl-6-(phenylethynyl)pyridine, MPEP & 50 μM LY341495) was tested. mGluR antagonists produce visible reduction of the slow current in both examples (blue). Data from all tested neurons are summarized in Figure 7b—the areas above filtered response traces, evoked by 200 Hz stimulation train, were measured, averaged, and plotted (mean \pm SEM) in a format similar to Figure 5b. mGlu receptor antagonists significantly reduced the response in 80% of V2M (4/5, $p < 0.001$, $p = 0.007$, $p = 0.017$, $p = 0.385$) and all S1 (3/3, $p < 0.001$, $p = 0.004$, $p = 0.011$) neurons.

4 | DISCUSSION

We used a combination of photostimulation, electrophysiology, and pharmacological agents to study the inputs to layer 1 neurons in two cortical areas of the mouse: barrel cortex of S1 and V2M. These areas were chosen as representatives of primary and higher order sensory areas. S1 is long established as the primary somatosensory cortex, and V2M has recently been identified as one of several higher order visual areas (Paxinos & Watson, 2008; Wang & Burkhalter, 2007). We found a similar pattern of inputs to layer 1 cells in both areas. These cells are innervated by strong driver inputs of cortical and thalamic origins (Cruikshank et al., 2012; Sherman, 2016) and they are targets of convergent inputs from other sources: these include GABAergic synapses from nearby layer 1 cells; monosynaptic glutamatergic, and monosynaptic and/or disynaptic GABAergic inputs from layers 2/3 (Jiang et al., 2013; Lee et al., 2015) and other lower layers, with considerable variability among these patterns for layer 1 neurons; and from a variety of subcortical modulatory centers, including the adrenergic, serotonergic, and nicotinic systems. Thus, processing by the layer 1 GABAergic neurons involves integration from multiple sources and regulation from classical neuromodulator systems.

4.1 | Inputs to layer 1 neurons running in layer 1

As noted in the Introduction, there has been great interest in afferents running in layer 1. Such afferents consist of inputs from the matrix thalamus (Jones, 1998) and major components of corticocortical connectivity, typically reflecting feedback from higher to lower areas, but occasionally contributing to feedforward processing (Cauller et al., 1998; D'Souza & Burkhalter, 2017; Marques et al., 2018). Such afferents have also been implicated in contextual and cross-modal processing, for example, underlying the modulation of visual response properties by auditory stimuli (Ibrahim et al., 2016; Roth et al., 2016). Indeed, prior studies have documented that layer 1 axons do target apical dendrites of pyramidal cells (Larkum, Zhu, & Sakmann, 1999; Petreanu, Mao, Sternson, & Svoboda, 2009) as well as layer 1 cells themselves (Cruikshank et al., 2012). Our data support the latter conclusion.

Glutamatergic synaptic responses of layer 1 neurons to layer 1 stimulation predominantly show paired-pulse depression (Figure 4), which in other circuits has been identified as driver inputs (Sherman, 2016). However, there is a small metabotropic glutamate receptor response to such stimulation (Figure 7), which signifies a modulator input (Sherman, 2016). The likely explanation for this is that the glutamatergic inputs running in layer 1 include both driver and modulator components, but that the large driver EPSCs showing depression obscure the smaller ones that would show facilitation, although it is also possible that these glutamatergic inputs may belong to a new type of synapses, rather than the traditional driver nor modulator class.

Stimulation of layer 1 axons also evoked slow currents that were inhibited by various antagonists of classical neuromodulators (Figures 5 and 6). The presence of nicotinic receptors on layer 1 interneurons has been previously reported (Christophe et al., 2002), suggesting cholinergic input, and the data presented here indicate the added presence of adrenergic and serotonergic inputs.

Clearly, because of the limited sample sizes used in this study, more detailed experiments are required to elucidate the subtypes and mechanisms involved for the metabotropic glutamate and neuromodulator receptors on these layer 1 neurons. Our results, however, do suggest a wide range of modulatory control of these layer 1 neurons by metabotropic glutamate receptors and long-range subcortical pathways.

4.2 | Inter- and intralaminar inputs to layer 1 neurons

Inputs to layer 1 cells from layers 2/3 have been previously reported (Chu et al., 2003; Lee et al., 2015; Wozny & Williams, 2011). We confirm such inputs here and show that these can be highly convergent. However, we also demonstrate that these layer 1 cells can also receive similar inputs from other lower layers. The patterns of such inputs, though usually spatially convergent, are diverse, and they lead to both direct excitation as well as monosynaptic or multisynaptic inhibition, the latter presumably via activation of nearby layer 1 neurons. The diversity here is not surprising, because layer 1 neurons have been known to show considerable variations in physiological and anatomical properties (Hestrin & Armstrong, 1996; Wozny & Williams, 2011; Zhou & Hablitz, 1996c), and the various patterns of the lower laminar inputs reported here may reflect different subclasses of layer 1 neurons and the circuit types involved.

5 | CONCLUSIONS

Our general understanding of the microcircuitry of cortex is that cells there are richly innervated by a wide range of converging inputs, including glutamatergic, GABAergic, and

classic modulatory sources, and the glutamatergic inputs involve a mix derived from local sources, other cortical areas, and often thalamus. Further, the common idea is that each cortical neuron integrates such inputs to regulate its firing properties. However, this view of cortical circuitry has not to date notably involved cells of layer 1, which have generally been ignored. The evidence we present here suggests that these layer 1 neurons are embedded in the same sort of circuitry involving the same general and diverse classes of inputs.

These layer 1 cells are strongly activated by layer 1 afferents (Cruikshank et al., 2012) and can profoundly affect responses of pyramidal cells via innervation of their apical dendrites (Larkum et al., 1999; Petreanu et al., 2009). In this regard, it is noteworthy that the only output of cortex that is organized to control behavior is represented by the very layer 5 pyramidal cells that extend apical dendritic tufts to within layer 1 (Sherman, 2016). It thus follows that understanding of the detailed circuitry affecting layer 1 cells is of clear importance to understanding cortical functioning.

ACKNOWLEDGEMENTS

This work was supported by the National Institutes of Health grants, NS094184 and EY022388.

CONFLICT OF INTEREST

The authors declare no competing financial interests.

DATA ACCESSIBILITY

Data are available from the corresponding author on request.

AUTHORS' CONTRIBUTIONS

The first author (YWL) performed the experiments. Both authors contributed equally to the experimental design, data analysis and preparation of the manuscript.

ORCID

Ying-Wan Lam  <https://orcid.org/0000-0003-3733-4242>

S. Murray Sherman  <https://orcid.org/0000-0002-1520-2778>

REFERENCES

- Avendano, C., Stepniewska, I., Rausell, E., & Reinoso-Suarez, F. (1990). Segregation and heterogeneity of thalamic cell populations projecting to superficial layers of posterior parietal cortex: A retrograde tracer study in cat and monkey. *Neuroscience*, *39*, 547–559. [https://doi.org/10.1016/0306-4522\(90\)90242-V](https://doi.org/10.1016/0306-4522(90)90242-V)
- Canepari, M., Nelson, L., Papageorgiou, G., Corrie, J. E., & Ogden, D. (2001). Photochemical and pharmacological evaluation of 7-nitroindolyl- and 4-methoxy-7-nitroindolyl-amino acids as novel, fast-caged neurotransmitters. *Journal of Neuroscience Methods*, *112*, 29–42. [https://doi.org/10.1016/S0165-0270\(01\)00451-4](https://doi.org/10.1016/S0165-0270(01)00451-4)
- Caulier, L. J., Clancy, B., & Connors, B. W. (1998). Backward cortical projections to primary somatosensory cortex in rats extend long horizontal axons in layer I. *Journal of Comparative Neurology*, *390*, 297–310. [https://doi.org/10.1002/\(ISSN\)1096-9861](https://doi.org/10.1002/(ISSN)1096-9861)
- Christophe, E., Roebuck, A., Staiger, J. F., Lavery, D. J., Charpak, S., Audinat, E. (2002). Two types of nicotinic receptors mediate an excitation of neocortical layer I interneurons. *Journal of Neurophysiology*, *88*, 1318–1327.
- Chu, Z., Galarreta, M., & Hestrin, S. (2003). Synaptic interactions of late-spiking neocortical neurons in layer I. *Journal of Neuroscience*, *23*, 96–102. <https://doi.org/10.1523/JNEUROSCI.23-01-00096.2003>
- Cox, C. L., & Sherman, S. M. (2000). Control of dendritic outputs of inhibitory interneurons in the lateral geniculate nucleus. *Neuron*, *27*, 597–610. [https://doi.org/10.1016/S0896-6273\(00\)00069-6](https://doi.org/10.1016/S0896-6273(00)00069-6)
- Cruikshank, S. J., Ahmed, O. J., Stevens, T. R., Patrick, S. L., Gonzalez, A. N., Elmaleh, M., & Connors, B. W. (2012). Thalamic control of layer 1 circuits in prefrontal cortex. *Journal of Neuroscience*, *32*, 17813–17823. <https://doi.org/10.1523/JNEUROSCI.3231-12.2012>
- Douglas, R. J., & Martin, K. A. (1991). A functional microcircuit for cat visual cortex. *Journal of Physiology*, *440*, 735–769. <https://doi.org/10.1113/jphysiol.1991.sp018733>
- D'Souza, R. D., & Burkhalter, A. (2017). A laminar organization for selective cortico-cortical communication. *Frontiers in Neuroanatomy*, *11*, 71. <https://doi.org/10.3389/fnana.2017.00071>
- Hestrin, S., & Armstrong, W. E. (1996). Morphology and physiology of cortical neurons in layer I. *Journal of Neuroscience*, *16*, 5290–5300. <https://doi.org/10.1523/JNEUROSCI.16-17-05290.1996>
- Ibrahim, L. A., Mesik, L., Ji, X. Y., Fang, Q., Li, H. F., Li, Y. T., ... Tao, H. W. (2016). Cross-modality sharpening of visual cortical processing through layer-1-mediated inhibition and disinhibition. *Neuron*, *89*, 1031–1045. <https://doi.org/10.1016/j.neuron.2016.01.027>
- Jiang, X., Wang, G., Lee, A. J., Stornetta, R. L., & Zhu, J. J. (2013). The organization of two new cortical interneuronal circuits. *Nature Neuroscience*, *16*, 210–218. <https://doi.org/10.1038/nn.3305>
- Jones, E. G. (1998). Viewpoint: The core and matrix of thalamic organization. *Neuroscience*, *85*, 331–345. [https://doi.org/10.1016/S0306-4522\(97\)00581-2](https://doi.org/10.1016/S0306-4522(97)00581-2)
- Lam, Y. W., Cox, C. L., Varela, C., & Sherman, S. M. (2005). Morphological correlates of triadic circuitry in the lateral geniculate nucleus of cats and rats. *Journal of Neurophysiology*, *93*, 748–757. <https://doi.org/10.1152/jn.00256.2004>
- Lam, Y. W., & Sherman, S. M. (2005). Mapping by laser photostimulation of connections between the thalamic reticular and ventral posterior lateral nuclei in the rat. *Journal of Neurophysiology*, *94*, 2472–2483. <https://doi.org/10.1152/jn.00206.2005>
- Lam, Y. W., & Sherman, S. M. (2007). Different topography of the reticulothalamic inputs to first- and higher-order somatosensory thalamic relays revealed using photostimulation. *Journal of Neurophysiology*, *98*, 2903–2909. <https://doi.org/10.1152/jn.00782.2007>
- Lam, Y. W., & Sherman, S. M. (2010). Functional organization of the somatosensory cortical layer 6 feedback to the thalamus. *Cerebral Cortex*, *20*, 13–24. <https://doi.org/10.1093/cercor/bhp077>

- Lam, Y. W., & Sherman, S. M. (2011). Functional organization of the thalamic input to the thalamic reticular nucleus. *Journal of Neuroscience*, *31*, 6791–6799. <https://doi.org/10.1523/JNEUROSCI.3073-10.2011>
- Lam, Y. W., & Sherman, S. M. (2015). Functional topographic organization of the motor reticulothalamic pathway. *Journal of Neurophysiology*, *113*, 3090–3097. <https://doi.org/10.1152/jn.00847.2014>
- Larkum, M. M., Zhu, J. J., & Sakmann, B. (1999). A new cellular mechanism for coupling inputs arriving at different cortical layers. *Nature*, *398*, 338–341. <https://doi.org/10.1038/18686>
- Lee, A. J., Wang, G., Jiang, X., Johnson, S. M., Hoang, E. T., Lante, F., ... Zhu, J. J. (2015). Canonical organization of layer 1 neuron-led cortical inhibitory and disinhibitory interneuronal circuits. *Cerebral Cortex*, *25*, 2114–2126. <https://doi.org/10.1093/cercor/bhu020>
- Marques, T., Nguyen, J., Fioreze, G., & Petreanu, L. (2018). The functional organization of cortical feedback inputs to primary visual cortex. *Nature Neuroscience*, *21*, 757–764. <https://doi.org/10.1038/s41593-018-0135-z>
- Paxinos, G., & Watson, C. (2008). *The mouse brain in stereotaxic coordinates*. Oxford, UK: Elsevier Science.
- Petreanu, L., Mao, T., Sternson, S. M., & Svoboda, K. (2009). The subcellular organization of neocortical excitatory connections. *Nature*, *457*, 1142–1145. <https://doi.org/10.1038/nature07709>
- Potjans, T. C., & Diesmann, M. (2014). The cell-type specific cortical microcircuit: Relating structure and activity in a full-scale spiking network model. *Cerebral Cortex*, *24*, 785–806. <https://doi.org/10.1093/cercor/bhs358>
- Roth, M. M., Dahmen, J. C., Muir, D. R., Imhof, F., Martini, F. J., & Hofer, S. B. (2016). Thalamic nuclei convey diverse contextual information to layer 1 of visual cortex. *Nature Neuroscience*, *19*, 299–307. <https://doi.org/10.1038/nn.4197>
- Rubio-Garrido, P., Perez-de-Manzo, F., Porrero, C., Galazo, M. J., & Clasca, F. (2009). Thalamic input to distal apical dendrites in neocortical layer 1 is massive and highly convergent. *Cerebral Cortex*, *19*, 2380–2395. <https://doi.org/10.1093/cercor/bhn259>
- Shepherd, G. M., Pologruto, T. A., & Svoboda, K. (2003). Circuit analysis of experience-dependent plasticity in the developing rat barrel cortex. *Neuron*, *38*, 277–289. [https://doi.org/10.1016/S0896-6273\(03\)00152-1](https://doi.org/10.1016/S0896-6273(03)00152-1)
- Sherman, S. M. (2016). Thalamus plays a central role in ongoing cortical functioning. *Nature Neuroscience*, *19*, 533–541. <https://doi.org/10.1038/nn.4269>
- Wang, Q., & Burkhalter, A. (2007). Area map of mouse visual cortex. *Journal of Comparative Neurology*, *502*, 339–357. [https://doi.org/10.1002/\(ISSN\)1096-9861](https://doi.org/10.1002/(ISSN)1096-9861)
- Winer, J. A., & Larue, D. T. (1989). Populations of GABAergic neurons and axons in layer I of rat auditory cortex. *Neuroscience*, *33*, 499–515. [https://doi.org/10.1016/0306-4522\(89\)90402-8](https://doi.org/10.1016/0306-4522(89)90402-8)
- Wozny, C., & Williams, S. R. (2011). Specificity of synaptic connectivity between layer 1 inhibitory interneurons and layer 2/3 pyramidal neurons in the rat neocortex. *Cerebral Cortex*, *21*, 1818–1826. <https://doi.org/10.1093/cercor/bhq257>
- Zhou, F. M., & Hablitz, J. J. (1996a). Layer I neurons of rat neocortex. I. Action potential and repetitive firing properties. *Journal of Neurophysiology*, *76*, 651–667. <https://doi.org/10.1152/jn.1996.76.2.651>
- Zhou, F. M., & Hablitz, J. J. (1996b). Layer I neurons of the rat neocortex. II. Voltage-dependent outward currents. *Journal of Neurophysiology*, *76*, 668–682.
- Zhou, F. M., & Hablitz, J. J. (1996c). Morphological properties of intracellularly labeled layer I neurons in rat neocortex. *Journal of Comparative Neurology*, *376*, 198–213. [https://doi.org/10.1002/\(ISSN\)1096-9861](https://doi.org/10.1002/(ISSN)1096-9861)
- Zhou, F. M., & Hablitz, J. J. (1997). Rapid kinetics and inward rectification of miniature EPSCs in layer I neurons of rat neocortex. *Journal of Neurophysiology*, *77*, 2416–2426. <https://doi.org/10.1152/jn.1997.77.5.2416>

How to cite this article: Lam Y-W, Sherman SM. Convergent synaptic inputs to layer I cells of mouse cortex. *Eur J Neurosci*. 2019;00:1–12. <https://doi.org/10.1111/ejn.14324>